BJR

https://doi.org/10.1259/bjr.20180492

Received: 31 May 2018 | Revised: 04 September 2018 | Accepted: 10 October 2018

Cite this article as:
Barisano G, Sepehrband F, Ma S, Jann K, Cabeen R, Wang DJ, et al. Clinical 7 T MRI: Are we there yet? A review about magnetic resonance imaging at ultra-high field. *Br J Radiol* 2019; **91**: 20180492.

REVIEW ARTICLE

Clinical 7 T MRI: Are we there yet? A review about magnetic resonance imaging at ultra-high field

[1,2]GIUSEPPE BARISANO, MD, [2]FARSHID SEPEHRBAND, PhD, [2]SAMANTHA MA, MS, [2]KAY JANN, PhD, [2]RYAN CABEEN, PhD, [2]DANNY J WANG, PhD, [2]ARTHUR W TOGA, PhD and [1,2]MENG LAW, MD

[1]Department of Radiology, Keck Medical Center of University of Southern California, Los Angeles, CA, USA
[2]Stevens Neuroimaging and Informatics Institute, University of Southern California, Los Angeles, CA, USA

Address correspondence to: Dr Giuseppe Barisano
E-mail: *giuseppe.barisano@loni.usc.edu*

ABSTRACT

In recent years, ultra-high field MRI (7 T and above) has received more interest for clinical imaging. Indeed, a number of studies have shown the benefits from the application of this powerful tool not only for research purposes, but also in realms of improved diagnostics and patient management. The increased signal-to-noise ratio and higher spatial resolution compared with conventional and high-field clinical scanners allow imaging of small anatomical detail and subtle pathological findings. Furthermore, greater spectral resolution achieved at ultra-high field allows the resolution of metabolites for MR spectroscopic imaging. All these advantages have a significant impact on many neurological diseases, including multiple sclerosis, cerebrovascular disease, brain tumors, epilepsy and neurodegenerative diseases, in part because the pathology can be subtle and lesions small in these diseases, therefore having higher signal and resolution will help lesion detection. In this review, we discuss the main clinical neurological applications and some technical challenges which remain with ultra-high field MRI.

INTRODUCTION

MRI is a non-invasive medical imaging technique that provides both structural and functional data on human brain. In addition to being a non-invasive procedure, the degree of anatomical detail imaged with MRI makes this technique the modality of choice for the diagnosis, treatment-planning, and follow-up in a number of neurological diseases.

Since the initial application of MRI in medical diagnostics in the mid-1980's, considerable efforts have been made by the scientific community in order to develop MR scanners with increasingly higher magnetic field strength (B_0) leading to enhanced signal-to-noise ratio (SNR), contrast-to-noise ratio (CNR), and exquisite spatial resolution. These advancements allowed the gradual transition from the first grainy images obtained with 0.3–0.6 T MR scanner to the current extensive use in clinical practice of conventional (1–1.5 T) and high-field (3 T) MRI, whose main benefits include not only improved imaging quality and diagnostic accuracy, but also faster acquisition.[1]

The first ultra-high field (UHF, or 7 T and greater) human MR image was acquired with the 8 T magnet at the Ohio State University in 1998.[2] The outcomes were exceptional and promising, resulting in the installations of numerous UHF research MR scanners worldwide, and in more recent years, the approval of clinical 7 T MRI scanners by the U.S. Food and Drug Administration (FDA). To date more than 80 human UHF MRI systems are operative, most of them with a magnetic field strength of 7 T.[3,4] Furthermore, after the FDA declared a non-significant risk for MRI up to 8 T in 2014,[5] an important step forward for UHF MRI in October 2017 was the Magnetom Terra (Magnetom Siemens Healthineers, Erlangen, Germany) becoming the first 7 T MRI system to obtain FDA 510(k) clearance for clinical use in the United States, limited to the examination of the head, upper and lower extremities.[6] This introduction will have remarkable repercussions in diagnostic radiology. In fact, the possibility to improve the spatial resolution reducing the size of the voxels thanks to the increased SNR of UHF, will enable clinicians to visualize smaller anatomical structures and greater detail of normal and pathological findings.

However, despite advances in magnet, coil, hardware and software technology, there are still limitations and technical challenges which need to be overcome.

In this article, we review the current literature and discuss the main clinical applications of UHF MRI in neuroimaging. Furthermore, we summarize the technical advantages and issues related with UHF MRI. A series of illustrative 7 T MRI examples is included.

References for this review were identified through searches of PubMed with the search terms "Utra-high field", "7T MRI", "7 Tesla MRI", "diffusion MRI", "Magnetic Resonance Spectroscopy", "BOLD fMRI" cross-referenced with the terms "Multiple Sclerosis", "cerebrovascular diseases", "stroke", "vessel imaging", "brain tumor", "epilepsy", "neurodegenerative diseases", "dementia", "Alzheimer", "Parkinson". Only articles published in English were reviewed. Reference lists of identified articles, book chapters, and authors' own references were also explored. Selection criteria were the novelty and importance in terms of potential clinical application of the reported results. Peer-reviewed articles published from 1967 until March 2018 have been included, in addition to two non-English historical references but with available translations dating back to the mid-1800s.

CLINICAL APPLICATIONS

There are a number of neurological diseases where UHF MRI has shown some benefit. These include multiple sclerosis (MS), cerebrovascular disease, neuro-oncology, epilepsy and neurodegenerative diseases. This may be because of the prevalence of these clinical entities, but also by the need to improve their diagnosis and clinical management through the identification and recognition of earlier disease and new imaging biomarkers. Furthermore, UHF MRI may play a role in helping neuroscientists, neurologists, neurosurgeons and neuroradiologists further insights on the pathophysiological mechanisms behind these conditions.

Multiple sclerosis

MS is the most common immune-mediated inflammatory demyelinating disorder affecting the central nervous system (CNS) and the leading cause of non-traumatic neurological disability in young adults in Northern America and Europe.[7] The diagnosis of MS is primarily clinical, but sometimes it may be challenging and further examinations are required, including radiological and laboratory tests. MRI is a helpful tool to support the diagnostic process, revealing the radiological dissemination in space and time of MS lesions; moreover, it may provide information relevant not only to clinical follow-up and monitoring of response to treatment, but also to a better understanding of MS pathophysiology.[8]

MS lesions or plaques typically appear as focal areas of hyperintensity on dual-echo (proton-density and T_2 weighted) and fluid-attenuated inversion-recovery (FLAIR) imaging on MRI, while post-gadolinium T_1 weighted images allow active lesions to be distinguished from inactive lesions, the first being enhanced on MRI unlike the latter. Even if 7 T MRI has not yet resulted in an earlier diagnosis, recent studies have demonstrated the main advantages of imaging at ultra-high field in MS. For instance, one of the first studies comparing 3 T and 7 T MRI in MS showed that on 7 T magnetization-prepared rapid acquisition gradient-echo (MPRAGE) a significantly higher number of focal MS lesions was detected in areas defined as "normal-appearing white matter" (NAWM) using standard clinical 3 T FLAIR: these abnormalities may contribute to the pathological changes that have been reported in NAWM.[9] Currently, it seems that there is increased sensitivity in the detection of gray matter lesions with UHF MRI[10,11] compared with 3 T MRI.

Another important benefit refers to cortical gray matter lesions' detection. According to the 2017 revision of the McDonald criteria for the diagnosis of MS, cortical lesions can be used to fulfill MRI criteria for dissemination in space.[12] Currently, this type of lesion is not easily identified with standard MRI protocols, due to the smaller volume of gray matter and lower levels of inflammation, but in the past years UHF MRI has demonstrated to provide an improved characterization of cortical lesions thanks to the increased spatial resolution and enhanced contrast.[13–16] A recent post-mortem verification study showed that the use of a multicontrast protocol including T_1 weighted, T_2 weighted, FLAIR, double-inversion recovery (DIR) and T2* at 7 T provided a cortical lesions detection rate more than two times higher as compared with 3 T; however, a considerable part of pathologically proven cortical lesions still remained undetected at 7 T MRI.[11]

Furthermore, UHF MRI has been increasingly used to investigate new possible hallmarks to accurately differentiate MS from its mimics. For example, various research groups have described central venules in MS lesions as a key element for the diagnosis of MS in challenging cases; this phenomenon, also named the "central vein sign" (CVS), was first reported by pathological studies in the 19th century,[17,18] and eventually confirmed using UHF MRI.[19,20] Even if the perivenular distribution of MS lesions is still detectable at T_2* weighted imaging with conventional and high-field scanners and high detection rate can be gained with optimized T_2* protocols,[21] the enhanced susceptibility effects around blood vessels achievable with UHF MRI result in reduced echo times and high SNR, which in turn can be used to generate more detailed imaging of the relationship between veins and MS lesions.[22] Indeed, Tallantyre et al demonstrated that the T_2* weighted imaging at 7 T has the highest sensitivity for central vein detection compared with 3 T,[22] and it can be helpful to distinguish between patients with demyelinating MS lesions and incidental asymptomatic white matter lesions in subjects without MS.[23] Moreover, several 3 and 7 T MRI studies showed that the proportion of the CVS in patients with MS is significantly higher compared with white matter lesions in patients with other neurological diseases, including neuromyelitis optica spectrum disorder, systemic autoimmune diseases, cerebral small vessel disease, Susac syndrome, and migraine.[24] These are typical differential diagnoses for MS and can sometimes be difficult to differentiate clinically and on MRI.

Another novel radiological MS feature is the peripheral paramagnetic rim revealed by MR susceptibility imaging (T_2* weighted magnitude and susceptibility-weighted phase images) in a subset of chronic lesions. Whether this finding is caused only by iron deposition or other MS pathological processes is

Figure 1. Axial SWI minIP Images at 7 T (left) and 3 T (right) of a healthy volunteer. The depiction of vessels is noticeably superior at UHF. The higher susceptibility and spatial resolution at 7 T allows detection of smaller vessels and the deoxyhenoglobin in veins which may be important for the detection of the "CVS" in the differential diagnoses of multiple sclerosis compare to other diseases which can cause demyelination such as neuromyelitis optica spectrum disorder, systemic autoimmune diseases, cerebral small vessel disease, Susac syndrome, and migraine, which typically woud not have the CVS. Resolution 7 T: 0.2 x 0.2 x 1.5 mm^3, scanning time = 5 min. Resolution 3 T: 0.9 x 0.9 x 1.2 mm^3, scanning time = 5 min. CVS, central vein sign; SWI, susceptibility-weighted imaging.

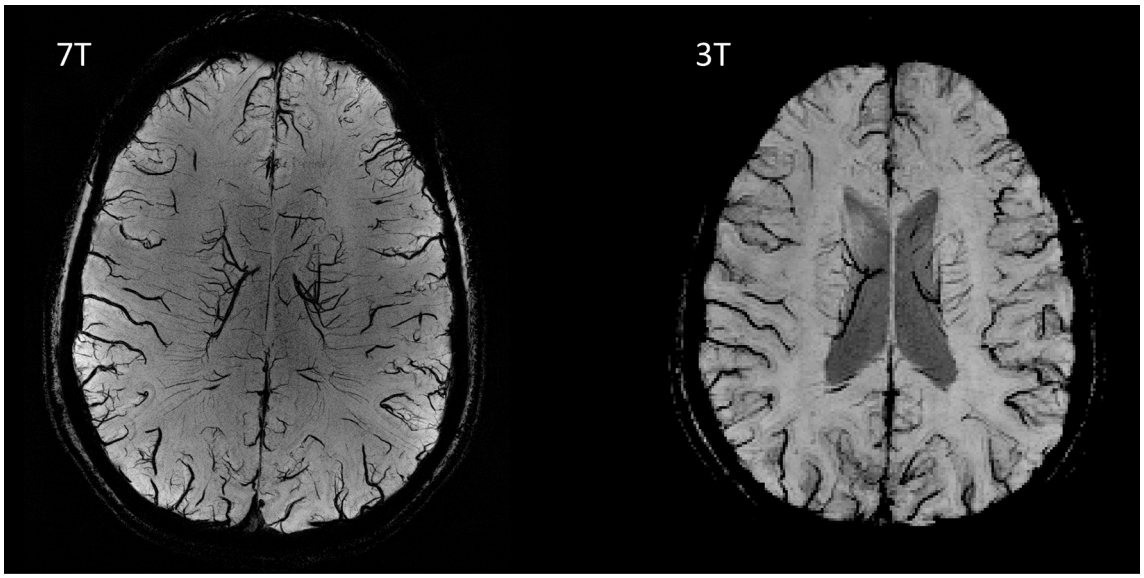

still debated, but in recent years relevant insights to its pathophysiological significance have been provided with UHF MRI.[20,25–27] Indeed, in addition to higher SNR and space resolution, phase images at UHF deliver contrast specific to field perturbations and show excellent contrast of local iron in white matter plaques, as susceptibility effects scale with field strength[25] (Figure 1).

Finally, a promising application of UHF MRI is MR Spectroscopy Imaging (MRSI). Indeed, the increased SNR results not only in improved spatial resolution for 7 T MRSI and shorter scan times, but also in enhanced spectral resolution (or chemical shift) compared with conventional and high-field 3 T clinical MRSI. The improved sensitivity and specificity of 7 T MRSI allow identification of metabolites with low concentration and offer improved discrimination of peaks of metabolites that otherwise overlap at lower field strength, such as glutathione (GSH), glutamate (Glu), glutamine (Gln), and myo-inositol (mI)[28] (Figure 2).

GSH is an indicator of oxidative status in the human brain and a spectral editing scheme called band selective inversion with gradient dephasing using proton MRSI has shown a significant reduction of GSH between the gray matter in MS patients and normal controls, indicating the potential of GSH as a marker for disease phenotype in MS.[30]

However, most of the results concerning these new potential MS hallmarks derive from small-cohort or single-centre studies; therefore large, prospective, multicenter trials are required to confirm their diagnostic role in MS.

In summary, the main advantages of UHF MRI for MS are the following: a better identification and morphological characterization of both white matter and gray matter lesions; the improved sensitivity to detection of new possible MS marker, including the CVS and the peripheral paramagnetic rim; the enhanced quantification of metabolites on MRSI. Although the role of these findings in MS diagnosis and clinical management still needs to be established, and the high cost of UHF MRI scanners makes unlikely this imaging technique to be routinely and widely used in clinical practice in the near future, we expect a growing application of UHF MRI in MS, not only for the validation and identification of new MS hallmarks in large clinical studies, but also to guide the development of novel diagnostic and therapeutic strategies at lower field.

Cerebrovascular disease

Worldwide, stroke is a leading cause of mortality and disability.[31] Both CT and MRI have a critical role in the diagnosis, treatment-planning, and follow-up in stroke patients: although CT has wide availability and faster acquisition time, MRI is the best technique to accurately visualize and characterize acute stroke on diffusion as well as both large and small vessels in the brain.[32] 3D time-of-flight (TOF)-MR angiography (MRA) is an established technique for imaging intracranial arteries thanks to the high signal contrast between the moving vascular protons and stationary protons. The T_1 relaxation times of tissues increase with field strength, so at UHF MRI, the longer T_1 values for tissue augment suppression of static background signal in TOF MRA increasing SNR and CNR in vessels with a resolution between 0.2 and 0.3 mm^3.[33] (Figure 3). This allows detection of intracranial

Figure 2. 7 T MR spectroscopy with metabolite peaks. The single voxel spectrum (2 cm isotropic) is located in the posterior cingulate cortex. The green box on top demonstrates the residual of the LCmodel fit[29] .Reliable concentrations have been demonstrated, with a standard deviation (%SD) inferior to 20% for most metabolites (Table). The improved sensitivity and specificity of 7 T MRS allow identification of metabolites with low concentration and discrimination of peaks of metabolites that overlap at lower field strength, such as glutamate (Glu), glutamine (Gln), and myo-inositol (mI). SD, standard deviation.

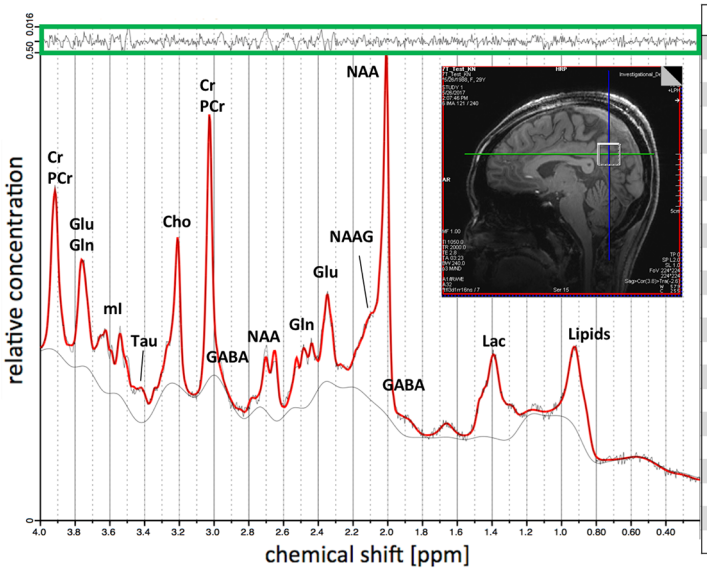

Conc.	%SD	/Cr+PCr	Metabolite
1.100	14%	0.170	Ala
1.554	21%	0.240	Asp
4.090	4%	0.631	Cr
2.393	7%	0.369	PCr
0.936	19%	0.144	GABA
2.387	18%	0.368	Glc
2.566	8%	0.396	Gln
5.428	4%	0.837	Glu
0.489	15%	0.075	GPC
0.739	10%	0.114	PCh
2.810	8%	0.433	Ins
0.348	48%	0.054	Lac
8.561	2%	1.320	NAA
1.397	8%	0.215	NAAG
0.193	21%	0.030	Scyllo
0.845	16%	0.130	Tau
0.000	999%	0.000	CrCH2
1.486	9%	0.229	Gua
1.228	3%	0.189	GPC+PCh
9.957	2%	1.536	NAA+NAAG
6.484	2%	1.000	Cr+PCr
7.994	4%	1.233	Glu+Gln

vessels with diameters less than 0.3 mm, including the small lenticulo-striate arteries, the pontine arteries, and the paramedian thalamic–subthalamic arteries, without ionizing radiation of invasive methods (digital subtraction angiography and CT angiography) or the intravenous administration of paramagnetic contrast agents such as gadolinium[34] (Figure 3).

Recently, a novel high-resolution black blood MRI technique has emerged for intracranial vessel wall imaging at 3 and 7 T using 3D turbo spin-echo (TSE) sequences with variable flip angles.[35–38] This T_1 weighted technique (also known as SPACE, Sampling Perfection with Application optimized Contrast using different angle Evolutions) offers an isotropic 0.5 mm spatial resolution,

Figure 3. Axial TOF-MRA MIP images at 7 T (left) and 3 T (right) of a healthy volunteer. An increased number of vessels is visible at UHF. Please note the increase conspicuity of the lenticulostriate arteries (arrows) arising from the M1 segement of the MCAs and the higher contrast seen in the insular branches of the MCAs (arrowheads). Resolution 7 T: 0.3 × 0.3 × 0.3 mm^3, 4 × 72 slices, scanning time = 4 × 2.23 min. MCAs, middle cerebral arteries; MRA, MR Angiography; MIP, maximum intensity projection; TOF,time of flight.

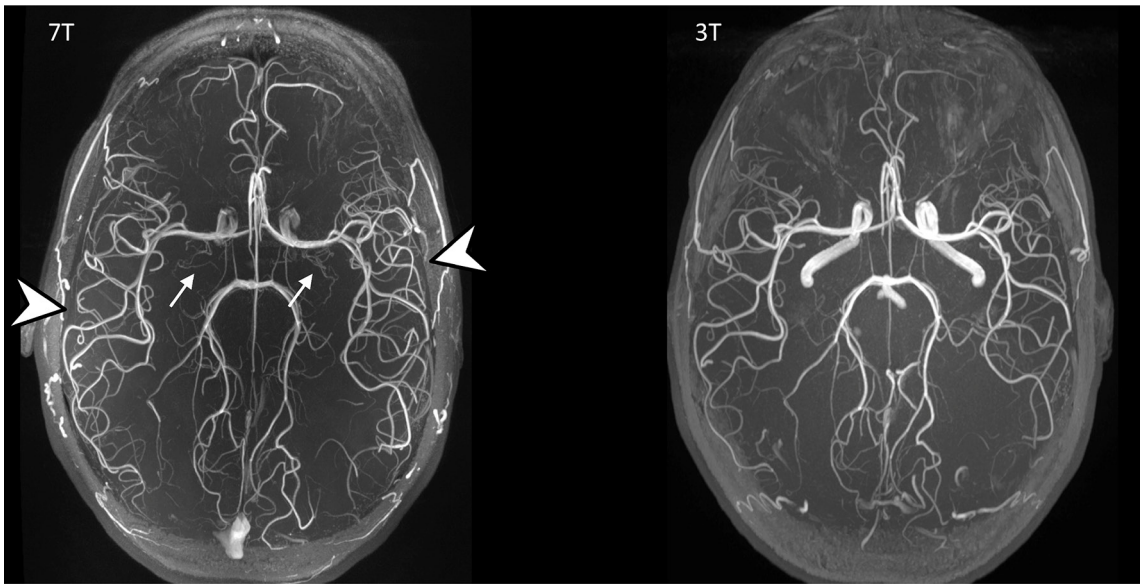

Figure 4. Thin minimum intensity projection across 10 mm slices from a 22-years-old healthy female subject at 3 and 7 T. Improved delineation of LSAs (white arrows) and reduced blurring, especially in the more distal vessels (arrowheads), can be appreciated at 7 T compared to 3 T. The visualization of these LSAs allows for visualization of normal vessels as well as the detection of possible pathologies such as arterial dissection and small LSA aneurysms (so called Charcot Bouchard microaneurysms). LSA, Lenticulostriate artery.

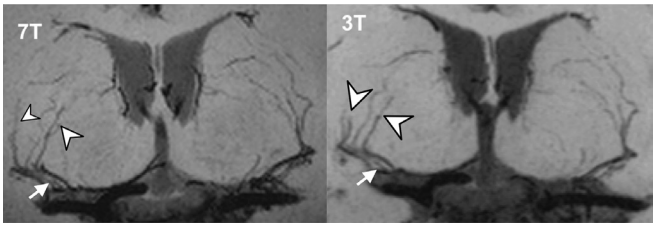

adequate flow suppression due to the long echo train, and near whole-brain coverage in less than 10 min; moreover, the excellent contrast between intracranial arterial wall and cerebrospinal fluid (CSF) allows better delineation of the vessel wall boundaries in vessels surrounded by CSF and to identify intracranial arterial disease.[37,38] At 7 T the substantial increase in SNR has led to significantly better 3D T_1 weighted SPACE image quality compared with 3 T, demonstrating an important potential for improved diagnostic performance[35,38] (Figure 4).

MRA and T_1-SPACE at UHF may provide novel clinically relevant non-invasive approaches to improve assessment of cerebrovascular diseases, including intracranial aneurysms,[39–41] vessel stenosis,[42,43] and microvascular pathological changes as well.[44]

Cerebral small vessel disease (SVD), a heterogeneous group of diseases affecting the perforating arterioles and capillaries in the brain, is the principal contributor to stroke and vascular cognitive impairment and dementia.[45,46] Features of SVD on MRI include brain atrophy, lacunes, enlarged perivascular space (PVS), white matter hyperintensities (WMH) and cerebral microbleeds. UHF has demonstrated potential clinical utility in better depicting these parenchymal lesions. T_1 weighted MPRAGE at 7 T offered superior visualization of the internal structure of stroke lesions and allowed improved detection of PVS compared with 3 T.[47] Also T_2 weighted TSE sequence at 7 T showed the same benefits, even though the authors observed more motion artifacts.[47] Comparable results in the identification of WMH were achieved with 3 and 7 T, yet better contrast between WMH and healthy tissue was observed at UHF.[47] Furthermore, a significantly higher number of cerebral microbleeds was identified at 7 T compared with both 3 and 1.5 T MRI.[48–50] Finally, the detection of cortical microinfarcts, another common SVD lesion not reliably visible on clinical MRI, was demonstrated to be feasible with 7 T scanners, providing new opportunities to investigate their role in cognitive function of SVD patients.[51] While it's more evident the relevance of these preliminary findings in research, further investigations are required to understand their real implications for routine clinical practice, as previous studies included a small number of patients.

Blood oxygenation level dependent functional MRI (BOLD fMRI) is another imaging technique showing significant advantages at UHF, derived from the increased SNR and susceptibility effects as well. The two main applications of BOLD fMRI at 7 T included the discrimination of the functional response between different cortical layers and mapping patterns of neuronal population activity for the first time even to submillimiter isotropic resolution.[52–55] Currently, the use of BOLD fMRI at UHF in clinical practice is still limited, but in the future it might be possible to use this tecnhique clinically, as for tracking cortical reorganization during rehabilitation in stroke patients.

In addition to the advances in UHF MRI systems, new image analysis and post-processing techniques have been established for segmentation and quantification of microvessels, allowing characterization of their morphologic details such as vessel length, tortuosity, caliber, and ultimately leading to identification of diseased microvessels.[56]

Neuro-oncology

Neuro-oncology is another important field where UHF MRI has shown encouraging promise for improving the diagnosis, treatment, and follow-up of brain tumors. For instance, increased spatial resolution may help in the detection of microvasculature in angiogenesis as well as small parenchymal and leptomeningeal metastases.

Moreover, the identification of metabolites with low concentration in 7 T MRSI is of remarkable interest for evaluating patients with glioma, the most common primary malignant brain tumor in adults.[57]

Ex vivo studies have demonstrated that mIn/total Choline (tCho) could be used to differentiate active tumor growth from proliferation of reactive astrocytes in response to treatment such as surgery or radiotherapy, and that mIn/tCho is able to distinguish the low grade gliomas upgraded to grade III from the recurrent grade IV lesions.[58,59] More recently, an *in vivo* study has verified differences in metabolite levels for regions of tumor vs normal brain, as well as between lesions.[60] Furthermore, Verma et al demonstrated the ability of two dimensional localized correlated MR spectroscopy at 7 T to detect 2-hydroxyglutarate as a biomarker for the *in vivo* determination of IDH mutation status in gliomas.[61] Based on these encouraging results, MRSI at UHF may represent a valuable non-invasive tool to accurately assess tumor classification and burden definition, leading to improvements in treatment planning and ultimately in patient prognosis and quality of life. The 2016 WHO classification of brain tumors made the identificaton of IDH mutation vs wildtype critically important for the subtyping of glioblastoma multiforme and the outcome.

Susceptibility-weighted imaging (SWI) and T_2^* at 7 T have been investigated to study the intratumoral microvascular structure in gliomas. Susceptibility contrast of para-magnetic substances, such as deoxyhemoglobin, is magnified at UHF and allows a superior depiction of veins and microhemorrhages.[62,63] This is particularly useful in brain tumors, where increased metabolism

leads to high deoxyhemoglobin levels and a better visualization of microvasculature on SWI. The analysis of tumor neovascularization is helpful to describe the grade of brain tumors and offers information on patient prognosis as well.[64,65] One study, *e.g.* suggested that the fractal dimension of intratumoral SWI pattern at 7 T MRI (indicative of microangioarchitecture and microbleedings) may effectively differentiate histopathological glial brain tumor grades.[66] Grabner et al explored the application of 7 T SWI to analyze changes in gliomas vascularization under antiangiogenic therapy, and they found that this task is especially appropriate for UHF MRI.[67] Another research group provided evidence for an improved depiction of tumor microvascularity at 7 T compared with 1.5 T, and showed increased vascularization from low- to high-grade gliomas.[68] Furthermore, the authors reported that the ring-shaped enhancement after contrast administration in a high-grade glioma is comparable at 1.5 and 7 T, but the central necrosis is emphasised at 7 T,[68] and this detailed characterization may be helpful to differentiate it from other similar radiological findings, such as necrotic metastases and cerebral abscesses. These studies demonstrate UHF MRI capabilities to provide useful information for grading gliomas and for monitoring tumor therapies.

Promising results of 7 T MRI for pituitary gland imaging have been achieved as well. Cushing's disease is the most common cause of adrenocorticotrophic hormone (ACTH)-dependent Cushing's syndrome, and is characterized by ACTH-producing adenoma located in the pituitary gland.[69] MRI is the preferred imaging technique to study pituitary gland in Cushing's Disease, but the majority of pituitary adenomas are microadenomas, and they result undetected in 36–63% of patients scanned with conventional clinical machines.[70,71] Therefore, further examinations, including invasive procedures such as inferior petrosal sinus sampling (IPSS), are often required to obtain a final diagnosis.[72] De Rotte et al demonstrated that more lesions were detected at 7 T MRI than 1.5 T, and the characterization of the lesions was more accurate at 7 T as well.[73] However, the authors reported the magnetic susceptibility effect related to the presence of air in the sphenoid sinus as a potential disturbing artifact for pituitary gland imaging.[73] Recently, Law et al reported a case of pituitary microadenoma that was visible at 7 T, but not easily seen on standard 1.5 T and even 3 T imaging studies[74] ; moreover, the 7 T MRI findings correlated with the results of IPSS[74] (Figure 5).

In the future, 7 T MRI may become a routine valuable diagnostic technique in patients with MRI negative Cushing's disease, possibly preventing the need of IPSS and improving the surgical planning and outcomes as well.

For brain metastases, the most common malignancy affecting the brain,[57] a study published in 2010 showed that the detection rate of cerebral metastases of bronchial carcinoma was almost equivalent on 1.5 and 7 T, but 20% more intralesional microhemorrhages were identified on SWI at 7 T.[75]

Finally, a recent study reported that in two patients with orbital choroidal melanoma uncertainty of optic nerve involvement at 3 T which was superiorly depicted at 7 T. This had relevant consequences for clinical management.[76]

Epilepsy

Epilepsy affects approximately 50 million people worldwide, and up to 30% of patients have disabling seizures that are refractory to antiepileptic drugs.[77] Focal cortical dysplasias (FCD) and mesial temporal sclerosis (MTS) are the two most common causes of drug-resistant focal epilepsy syndromes, and in these cases resective surgery is the most effective treatment for patients to become seizure-free, improving their quality of life.[78] The success rate of epilepsy surgery is critically related to the ability to identify a structural lesion on MRI; indeed, in patients with an MRI-detectable lesion, seizure freedom after surgery is achieved in around 70% of cases, compared with 40% when MRI is negative.[79] Currently, a significant proportion (almost 25%) of surgical candidates demonstrates no relevant structural MRI abnormalities with conventional scanners, so the introduction of more higher resolution imaging techniques and diagnostic tools is needed, not only for a better surgical outcome, but also for facilitating the pre-surgical planning without invasive procedures, such as intracerebral electrode implantation.[80] De Ciantis et al reported structural abnormalities detected at 7 T MRI and not previously identified with 1.5 and/or 3 T MRI in 6 out of 21 patients (29%) with focal epilepsy.[81]

Figure 5. Postcontrast T_1-weighted MR images at 7 T (left), 3 T (middle), and 1.5 T (right). 7 T imaging demonstrates what appears to be an 8-mm right-sided hypoenhancing pituitary microadenoma (white arrow), not visible at 3 and 1.5 T. From Law et al., JNS 2018[74] (https://doi.org/10.3171/2017.9.JNS171969), permission from Elsevier.

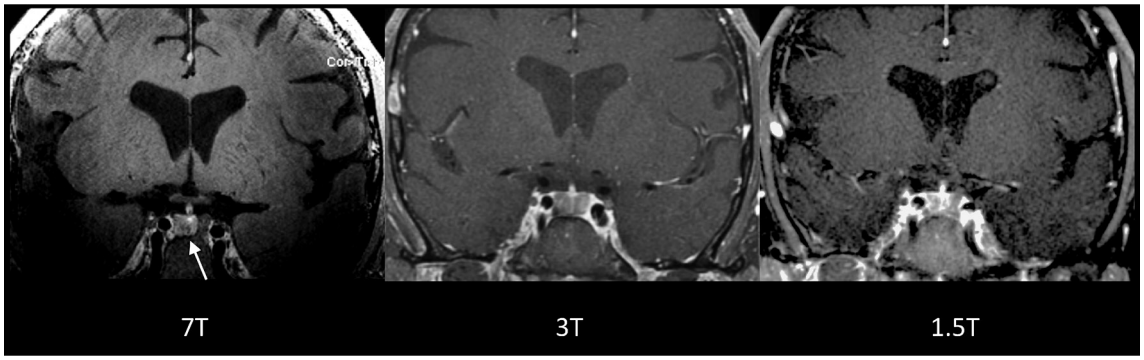

Specifically, two sequences showed the advantage of 7 T: (1) the 2D T_2* weighted dual-echo gradient-recalled echo (GRE) targeted for localization of the seizure onset zone, improving the evaluation of the different components and even layers within the cortex, and (2) the 3D magnetization-prepared (MP)-FLAIR sequence.[81] In a previous study by the same group, 7 T MRI was found to reveal more anatomic detail compared with 3 T in a group of 10 patients with polymicrogiria, a malformation of the cerebral cortex characterized by an excessive number of abnormally small gyri resulting in a large spectrum of possible symptoms, including refractive epilepsy.[82,83] Thanks to higher resolution 7 T MRI, the detection of bilateral involvement was demonstrated in four patients who had been classified as having only unilateral polymicrogyria at 3 T[82] ; moreover, 3D susceptibility-weighted angiography (SWAN) at 7 T revealed numerous dilated cortical veins not visible at 3 T, suggesting a role for vascular dysgenesis in the pathogenesis of polymicrogyria.[82]

Another recent paper investigated the role of PVS in the brain as a new potential biomarker for the altered macrophage activity associated with seizure onset at 7 T MRI.[84] The authors used axial T_2 weighted TSE sequences to analyze and quantify PVS in 21 subjects with focal epilepsy and 17 healthy volunteers: PVS distribution was found to be significantly more asymmetric in epilepsy patients, and the region of maximum asymmetry was within the suspected seizure onset zone in 72% of cases.[84] Thanks to improved contrast and resolution, the depiction of PVS, also known as Virchow-Robin spaces, is significantly improved at UHF and greater details can be visualized compared with 3 T MRI.[47]

Springer et al demonstrated a higher diagnostic confidence for MTS at 7 T compared with 3 T, primarily due to the higher spatial resolution in the coronal T_2 TSE sequence, even if the difference did not reach statistical significance.[85] In their work, they were able to identify which hippocampal subfields were affected, toward assignment of the histologic subtype according to the ILAE consensus classification of hippocampal sclerosis.[86] The 7 T coronal TSE sequence demonstrated the best conspicuity for the depiction of hippocampal area, as the susceptibility artifacts commonly seen in the skull base region did not significantly affect the imaging of hippocampus.[85] However, the coil-related signal decrease in the posterior fossa as well as the higher B_1 inhomogeneity affecting imaging at UHF are still a problem.[85]

Finally, UHF MRI may potentially provide further insights into the study of patients with cryptogenic seizures, that traditionally represent around 30% of all epilepsies.[87] For instance, previous studies have shown that SWI and T_2*-weighted GRE sequences at 7 T were able to identify more cerebral cavernous malformations and possibly associated developmental venous anomalies compared with 3 and 1.5 T clinical scanners, respectively, and these findings may have important implications for diagnostic and therapeutic purposes as well.[88,89]

Neurodegenerative diseases

Alzheimer's Disease (AD) is the most common cause of cognitive decline in the elderly.[90] A dramatic rapid increase in population numbers of older people worldwide is expected in the next decades thanks to the progress made in medicine and social conditions.[91] Consequently, the incidence and prevalence of AD and other dementias will increase, with huge costs to society and healthcare systems.[91] Despite the efforts made by the scientific community to better understand the neuropathology in AD, the pathophysiological mechanisms of this devastating disorder are still not well-known and therapies that effectively reverse or slow AD progression are desperately needed.[92]

Figure 6. Hippocampal subfield imaging with high resolution coronal T_2 weighted contrast at 3 and 7 T. 3 T image: in-plane resolution: 400 μm, slice thickness: 2 mm, sequence: BLADE[98] , no repetition, total acquisition time: 10 mins. 7 T image: in-plane resolution: 300 μm, slice thickness: 2 mm, sequence: TSE, 4 averages and 2 concatenations, total acquisition time: 11 mins. Note that Fimbria (white arrow), Alveus (arrowhead), and Stratum layers were resolved at 7 T. SE, turbo spin echo.

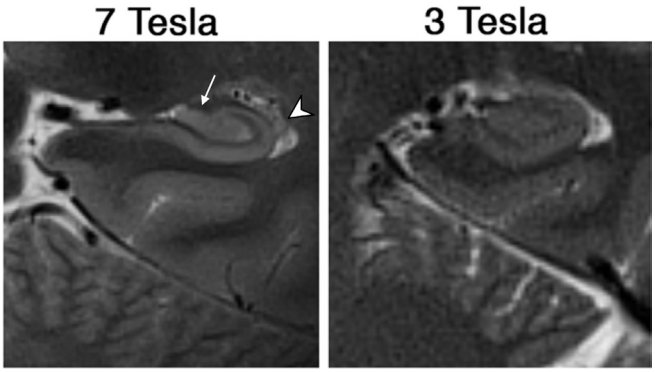

Neuroimaging approaches with UHF MRI may offer novel means to investigate AD. For example, previous studies showed that the sensitivity of 7 T MRI in detecting changes in the hippocampal strata is superior at 7 T compared with 1.5 and 3 T.[93,94] The stratum radiatum and lacunosum-moleculare of the Cornu Ammonis' field 1 (CA1) have been shown to be thinner in mild AD patients than in controls, without any changes in the stratum pyramidale of CA1(93). Furthermore, the use of new segmentation techniques at 7 T allows superior quantitation of hippocampal subfields volumes because of the increase CNR, SNR, and spatial resolution. Investigators have demonstrated a decrease in the volume of all subfields (except CA2) and the enthorinal cortex in AD patients.[95,96] More recently, Sepehrband et al were able to image the hippocampal subregions, including the stratum pyramidal of rostral CA3, the alveus, and even the endfolial pathway[97] (Figure 6).

The investigation of T_2* hypointensities has taken advantage of UHF MRI as well. Van Rooden et al reported that 3D T_2* sequences at 7 T demonstrated abnormalities in human brain specimens with AD and cerebral amyloid angiopathy (CAA), including hypointense foci and/or diffuse grainy inhomogenities of the cortex[99] ; furthermore, iron deposits were co-located with amyloid deposits on histology.[99] According to the authors, these foci may represent a neuroimaging biomarker for *in vivo* detection of amyloid-β plaques, facilitating the diagnosis of AD and CAA.[99] However, another *ex vivo* study using 7 T MRI

showed that the hypointense foci were primarily located within the subiculum of AD specimens, suggesting that they may be more related to activated iron-containing microglia rather than amyloid deposits.[100]

Recently, the role played by PVS as a clearance system of cerebral metabolic products and its implication for neurodegeneration have been investigated. The UHF MRI enabled to study these structures with a quantitative approach and explore their possible influence in dementia. One post-mortem study showed a clear positive association between dilation of juxtacortical PVS in a given region revealed on 7 T MRI and higher amyloid-β deposition in the same area of five cerebral AD specimens.[101] Furthermore, Cai et al used the T_2-SPACE sequence at 7 T to compute the total PVS volume in five AD patients compared with three healthy controls, and they reported that PVS density in centrum semiovale was significantly higher in AD patients.[102]

Finally, new evidence suggests that subtle white matter changes begin in preclinical AD and can be measured by diffusion tensor imaging (DTI), an advanced diffusion-weighted MRI (DWI) modeling technique for assessing the microstructure of the brain.[103] Compared to 3 T, the higher spatial resolution and reduction of partial volume effects at 7 T enables better separation of fiber bundles in white matter and cortical regions as well[104,105] (Figures 7 and 8). A multipurpose multishell DWI sequence was reported to fit a clinically acceptable acquisition time frame of ~10 min.[109]

Parkinson's Disease (PD) is the second most common neurodegenerative disorder after AD,[110] and it is clinically characterized by motor symptoms, such as resting tremors and rigidity,[111] and pathologically by α-synuclein intracellular inclusions, resulting in Lewy bodies formation and loss of neurons in substantia nigra (SN) and elsewhere.[112] Several 7 T studies of PD have demonstrated the advantages of UHF MRI in comparison with conventional scanners imaging, reporting improvements in diagnostic accuracy and treatment planning. For instance, Cosottini et al showed that 3D multiecho SWI sequence at 7 T was able to precisely characterize the SN and its internal organization, leading to near-perfect discrimination of PD patients from age-matched healthy subjects.[113] Deep brain stimulation (DBS) of the subthalamic nucleus (STN) is an effective surgical therapy for patients with advanced PD,[114] however in some cases this treatment is not able to provide relief of parkinsonian symptoms, and possible side effects may occur as well.[115] One of the most important factors for a successful outcome is the accuracy of targeting: the electrode should be placed preferentially in the motor region of the STN in order to exclude or minimize the stimulation of the non-motor zone.[115] Plantinga et al demonstrated that tractography-based technique at UHF MRI may facilitate the identification of the motor zone of the STN in individual patients, allowing for more optimized patient-specific surgical planning.[116,117] Although 7 T MRI can provide significantly improved visualization of STN, geometric distortion (or pixel shifts) is more pronounced with increasing field strength, representing a critical challenge for DBS.[118] Nonetheless, different approaches, including distortion correction and image reconstruction techniques such as QSM, have recently shown encouraging results and might be useful to address this issue.[119,120]

CURRENT CHALLENGES

Current major challenges in UHF MRI include inhomogeneity in the main magnetic field (B_0) and the applied radiofrequency (RF) field (B_1), increased specific absorption rate (SAR), and the increased sensitivity to motion artifacts.

B_0 inhomogeneities are related to the magnetic susceptibility difference between air cavities in the human skull and brain tissue. This effect scales linearly with the magnetic field strength, leading to significant distortion and non-uniformity of signal intensity in images obtained at UHF, especially when very fast image acquisition techniques, such as echo planar imaging (EPI), are applied. Moreover, the metabolite peaks in MRSI may be affected by spectral shifts and intravoxel broadening with potential peaks overlapping; also, the suppression of water and fat is more challenging due to widening of the water and fat spectral peaks. The implementation of higher order shimming has shown to significantly reduce the B_0 inhomogeneities, but unfortunately most human 7 T MR scanners are equipped with only second degree shims.[121] Moreover, parallel imaging technique, such as generalized auto-calibrating partially parallel acquisitions (GRAPPA), in combination with readout-segmented EPI is able to reduce susceptibility-related distortions and improve the image quality thanks to the decrease of the acquired k-space data and a restricted field of view (FOV).[122]

As the magnetic field strength increases, the Larmor wavelength for protons in the human head decreases and the RF wavelength in tissues becomes smaller than anatomical structures. The non-uniformity of B_1 derives from the interaction between the asymmetric and inhomogeneous human head, the RF coil, and the excitation sources.[123] This effect leads to changes in CNR and flip angles across the FOV, and a reduction of SNR from the center of the brain to the periphery and in the head-foot direction as well. Solutions to deal with B_1 inhomogeneities have been proposed. For instance, adiabatic RF pulses, modulating frequency and amplitude of the applied RF field above the adiabatic threshold, are relatively insensitive to B_1 inhomogeneities, allowing to uniformly rotate the net magnetization with a constant flip angle, and improving the outer-volume suppression.[124] Another solution is the employment of parallel excitation arrays with multiple independent transmit coils, in order to create a more uniform B_1 field by modelling the RF waveform and the RF pulse sequences on each specific channel.[125] B_1 non-uniformities represents a significant challenge not only for UHF imaging of the brain, but especially for spinal cord imaging, as the presence of vertebral bodies further exacerbates B_1 inhomogeneites. Despite many different solutions have been proposed, the optimal coil configuration for 7 T spinal cord imaging is not yet known and more efforts are needed to address this technical challenge.[126]

SAR represents the measurement in watts per kilograms of RF power delivered during the scan to human tissues, with their subsequent heating. SAR increases roughly quadratically with

Figure 7. Color fractional anisotropy (A, B, D, E) and DTI principal direction of diffusion (C, F) maps from the Human Connectome Project. 7 T (A, B, and C, 1.05 mm^3 isotropic resolution) and 3 T (D, E, and F, 1.25 mm^3 isotropic resolution) from the same subject. Red, green and blue indicate regions with diffusivities oriented primarily laterolateral, ventrodorsal, and rostrocaudal, respectively. Improved resolution allows identification of fiber tracks (red arrows and yellow arrows in B) which are faintly visible at 3 T. Note increased B1 + inhomogeneity resulting in signal loss in temporal lobe regions at 7 T (white arrows in A).

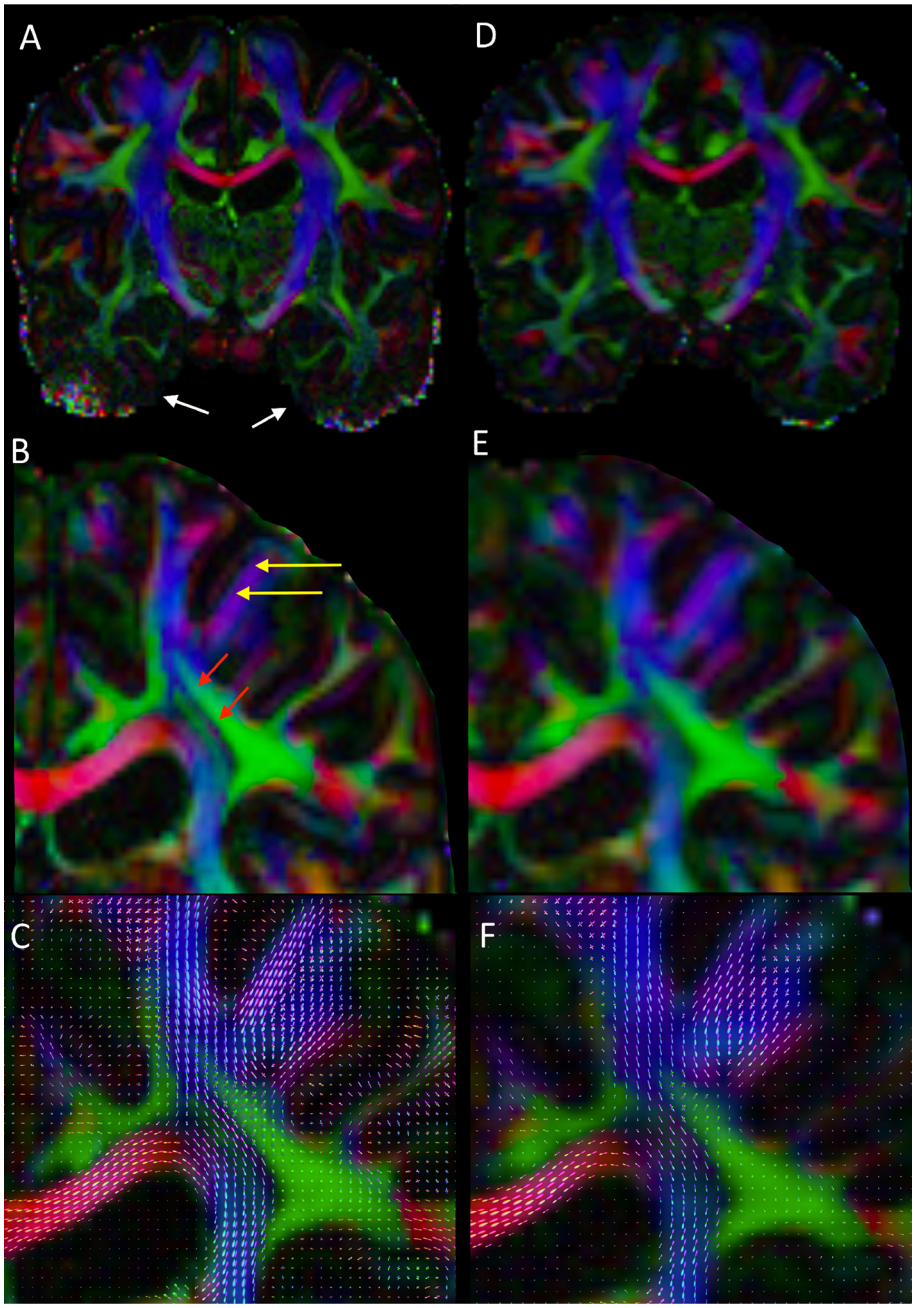

the B_0, and other influencing factors include the total amount and frequency of RF pulses: sequences using large and very rapid RF pulses, such as spin-echo and TSE, lead to higher SAR, while GRE sequences (except TOF) typically result in lower SAR. FDA sets regulatory limits for RF safety and all MRI scanners are able to compute an estimate of the SAR before each acquisition in order to guarantee all subjects are safe during the scan. Methods to lower SAR include the use of parallel imaging techniques, the reduction of flip angles and number of echoes in multiecho acquisition, and the lengthening of TR. Longer TRs naturally result in longer acquisition times. This is still sometimes a challenge at 7 T.

Image artifacts such as ringing, ghosting, and blurring caused by motion of the subject during the MRI exam constitute a significant problem both for clinical 1.5 and 3 T MRI, and for 7 T MRI as well. Although imaging at UHF resulted in faster acquisition, the higher resolution derived from improved SNR

Figure 8. Fiber orientation glyphs (A, B) and tractography reconstructions (C, D) from the Human Connectome Project. 7 T (A, C: 1.05 mm^3 isotropic resolution) and 3 T (B, D: 1.25 mm^3 isotropic resolution) from the same subject. Fiber orientations were estimated using FSL BEDPOSTX[106] and visualized using the Quantitative Imaging Toolkit (QIT);[107] the 7 T data shows improved modeling of cortical fiber orientations (blue arrow). Tractography models of the superior longitudinal fasciculus I were created using deterministic streamline tractography in QIT[107,108]; the 7 T data shows improved reconstruction of orbitofrontal connections of the pathway in both hemispheres (white arrow).

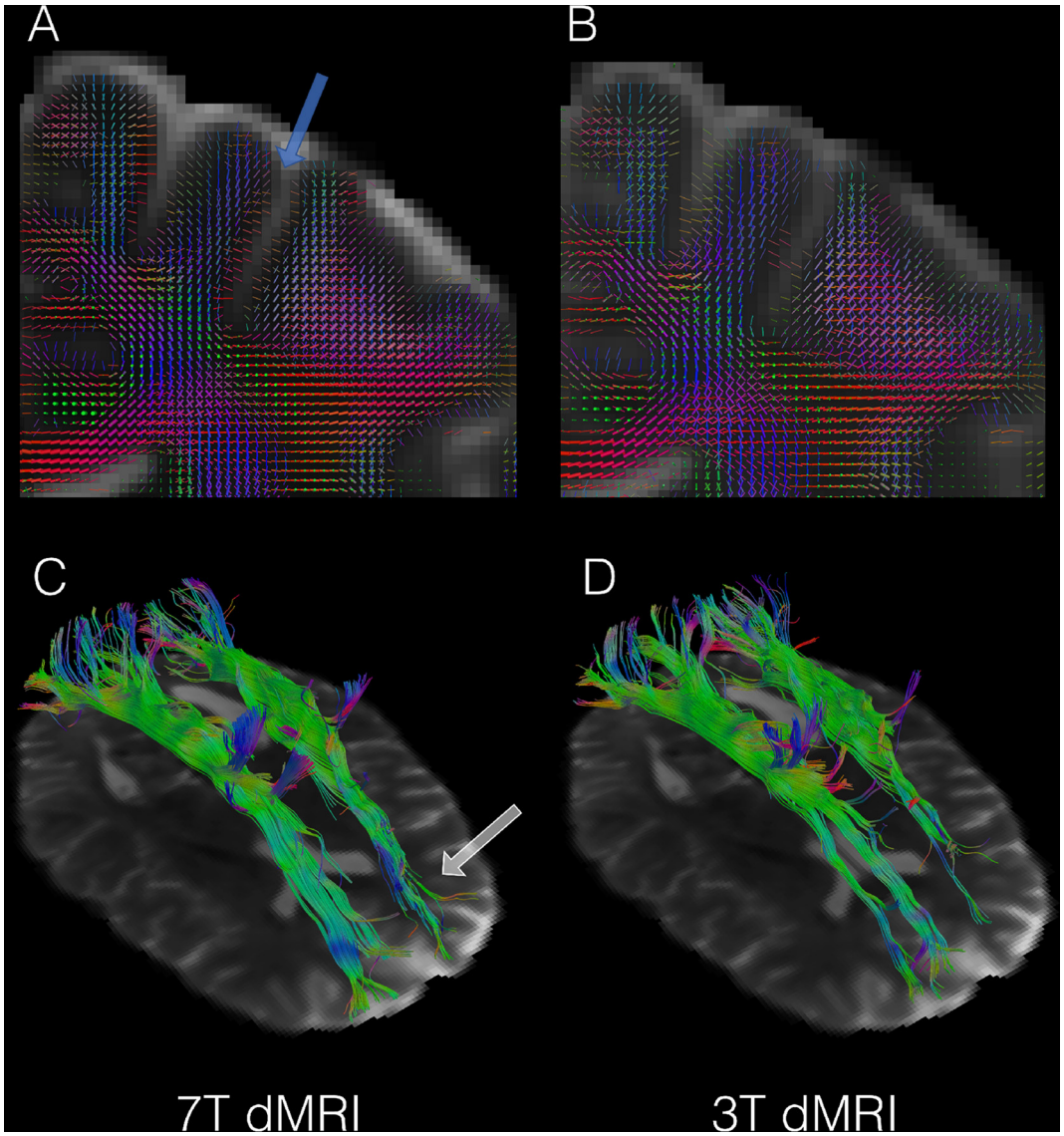

lead to increased sensitivity to motion.[127] Even with co-operative subjects, the presence of physiological spontaneous movements, including breathing, heartbeating, and muscle relaxation, may cause motion artifacts.[128] Different motion correction procedures exist, including post-processing retrospective techniques and real-time prospective methods: the first is applied after the data have been acquired, while the latter approach detects the subject motion during the scan and dynamically adjusts the imaging protocol tracking the motion to reduce the artifacts. For instance, prospective motion correction system (Kineticor, HI), using an optical tracking system composed by a single camera and a moiré phase tracking marker to obtain head motion information in real time, has recently shown to be feasible and effective in reducing the artifacts caused by physiological movements at 7 T MRI.[129]

Another limiting factor that impacts both research and clinical utilization of 7 T MRI is related to biomedical implants. Currently, relatively few implants have undergone proper testing at 7 T MR scanner, precluding a significant portion of subjects and patients from taking advantage of UHF MRI.[130–132]

Moreover, although many 7 T protocols have demonstrated to provide images with a significantly higher level of details compared with 3 T MRI, increased resolution is often concomitant with increased image-encoding burden that can cause long

scan times, a condition not always acceptable in clinical setting. For this reason, new acquisition methods, including RF pulse design schemes and parallel imaging approaches such as simultaneous multislice and volumetric 3D imaging, have been developed in order to obtain high-quality images over the entire brain within a relatively short time-frame.[133]

CONCLUSION

7 T MRI is set to become a clinical tool in addition to numerous research applications. Several studies have demonstrated that the increased spatial resolution and SNR may have significant clinical implications for the diagnosis, treatment, and follow-up of patients in a number of neurological diseases. However, further studies comparing conventional, high-field, and UHF MRI are needed in order to verify on a larger scale the diagnostic and therapeutic advantages reported in previous studies discussed in this paper. Moreover, the development of new imaging, post-processing, and analyses techniques is desirable not only to overcome the technical challenges, but also to maximize the image quality attainable at UHF MRI so as to demonstrate current and discover future clinical applications.

DISCLOSURE

The authors report no conflict of interest concerning the material or methods used in this study or the findings specified in this paper.

REFERENCES

1. Alvarez-Linera J. 3T MRI: Advances in brain imaging. *Eur J Radiol* 2008; **67**: 415–26. doi: https://doi.org/10.1016/j.ejrad.2008.02.045
2. Robitaille P-ML, Abduljalil AM, Kangarlu A, Zhang X, Yu Y, Burgess R, et al. Human magnetic resonance imaging at 8 T. *NMR Biomed* . 1998; **11**: 263–5. doi: https://doi.org/10.1002/(SICI)1099-1492(199810)11:6<263::AID-NBM549>3.0.CO;2-0
3. Kraff O, Fischer A, Nagel AM, Mönninghoff C, Ladd ME. MRI at 7 Tesla and above: demonstrated and potential capabilities. *J Magn Reson Imaging* 2015; **41**: 13–33. doi: https://doi.org/10.1002/jmri.24573
4. Park C-A, Kang C-K, Kim Y-B, Cho Z-H. Advances in MR angiography with 7T MRI: From microvascular imaging to functional angiography. *Neuroimage* . 2018; **168**(March): 269–78. doi: https://doi.org/10.1016/j.neuroimage.2017.01.019
5. US Food and Drug Administration (FDA). Criteria for significant risk investigations of magnetic resonance diagnostic devices. 2014. Available from: https://www.fda.gov/RegulatoryInformation/Guidances/ucm072686.htm [October 2018].
6. US Food and Drug Administration (FDA). FDA clears first 7T magnetic resonance imaging device. 2017*FDA News Release*. Available from: https://www.fda.gov/NewsEvents/Newsroom/PressAnnouncements/ucm580154.htm [October 2018].
7. Noseworthy JH, Lucchinetti C, Rodriguez M, Weinshenker BG, Sclerosis M. Multiple Sclerosis. *N Engl J Med Overseas Ed* 2000; **343**: 938–52. doi: https://doi.org/10.1056/NEJM200009283431307
8. Filippi M, Rocca MA. MR imaging of multiple sclerosis. *Radiology* 2011; **259**: 659–81. doi: https://doi.org/10.1148/radiol.11101362
9. Mistry N, Tallantyre EC, Dixon JE, Galazis N, Jaspan T, Morgan PS, et al. Focal multiple sclerosis lesions abound in 'normal appearing white matter'. *Mult Scler* 2011; **17**: 1313–23. doi: https://doi.org/10.1177/1352458511415305
10. de Graaf WL, Kilsdonk ID, Lopez-Soriano A, Zwanenburg JJM, Visser F, Polman CH, et al. Clinical application of multi-contrast 7-T MR imaging in multiple sclerosis: increased lesion detection compared to 3 T confined to grey matter. *Eur Radiol* 2013; **23**: 528–40. doi: https://doi.org/10.1007/s00330-012-2619-7
11. Kilsdonk ID, Jonkman LE, Klaver R, van Veluw SJ, Zwanenburg JJM, Kuijer JPA, et al. Increased cortical grey matter lesion detection in multiple sclerosis with 7 T MRI: a post-mortem verification study. *Brain* 2016; **139**: 1472–81. doi: https://doi.org/10.1093/brain/aww037
12. Thompson AJ, Banwell BL, Barkhof F, Carroll WM, Coetzee T, Comi G, et al. Diagnosis of multiple sclerosis: 2017 revisions of the McDonald criteria. *Lancet Neurol* 2018; **17**: 162–73. doi: https://doi.org/10.1016/S1474-4422(17)30470-2
13. Kollia K, Maderwald S, Putzki N, Schlamann M, Theysohn JM, Kraff O, et al. First clinical study on ultra-high-field MR imaging in patients with multiple sclerosis: Comparison of 1.5T and 7T. *American Journal of Neuroradiology* 2009; **30**: 699–702. doi: https://doi.org/10.3174/ajnr.A1434
14. Kangarlu A, Bourekas EC, Ray-Chaudhury A, Rammohan KW. Cerebral cortical lesions in multiple sclerosis detected by MR imaging at 8 Tesla. *Am J Neuroradiol* 2007; **28**: 262–6.
15. Pitt D, Boster A, Pei W, Wohleb E, Jasne A, Zachariah CR, et al. Imaging Cortical Lesions in Multiple Sclerosis With Ultra–High-Field Magnetic Resonance Imaging. *Arch Neurol* 2010; **67**: 812–8. doi: https://doi.org/10.1001/archneurol.2010.148
16. Mainero C, Benner T, Radding A, van der Kouwe A, Jensen R, Rosen BR, et al. In vivo imaging of cortical pathology in multiple sclerosis using ultra-high field MRI. *Neurology* 2009; **73**: 941–8. doi: https://doi.org/10.1212/WNL.0b013e3181b64bf7
17. Rindfleisch E. Histologisches detail zu der grauen degeneration von gehirn und rückenmark. (Zugleich ein Beitrag zu der Lehre von der Entstehung und Verwandlung der Zelle.). *Arch für Pathol Anat und Physiol und für Klin Med [Internet]* 1863; **26**: 474–83.
18. Charcot JM. Histologie de la sclerose en plaques. *Gaz des Hop* 1868; **41**: 554–66.
19. Tallantyre EC, Brookes MJ, Dixon JE, Morgan PS, Evangelou N, Morris PG. Demonstrating the perivascular distribution of MS lesions in vivo with 7-Tesla MRI. *Neurology* 2008; **70**: 2076–8. doi: https://doi.org/10.1212/01.wnl.0000313377.49555.2e
20. Hammond KE, Metcalf M, Carvajal L, Okuda DT, Srinivasan R, Vigneron D, et al. Quantitative in vivo magnetic resonance imaging of multiple sclerosis at 7 Tesla with sensitivity to iron. *Ann Neurol* 2008; **64**: 707–13. doi: https://doi.org/10.1002/ana.21582
21. Dixon JE, Simpson A, Mistry N, Evangelou N, Morris PG. Optimisation of T2*-weighted MRI for the detection of small veins in multiple sclerosis at 3 T and 7 T. *Eur J Radiol* . 2013; **82**: 719–27.

22. Tallantyre EC, Morgan PS, Dixon JE, Al-Radaideh A, Brookes MJ, Evangelou N, et al. A comparison of 3T and 7T in the detection of small parenchymal veins within MS lesions. *Invest Radiol* . 2009; **44**: 491–4. doi: https://doi.org/10.1097/RLI.0b013e3181b4c144
23. Tallantyre EC, Dixon JE, Donaldson I, Owens T, Morgan PS, Morris PG, et al. Ultra-high-field imaging distinguishes MS lesions from asymptomatic white matter lesions. *Neurology* 2011; **76**: 534–9. doi: https://doi.org/10.1212/WNL.0b013e31820b7630
24. Sati P, Oh J, Constable RT, Evangelou N, Guttmann CRG, Henry RG, et al. The central vein sign and its clinical evaluation for the diagnosis of multiple sclerosis: a consensus statement from the North American Imaging in Multiple Sclerosis Cooperative. *Nat Rev Neurol* 2016; **12**: 714–22. doi: https://doi.org/10.1038/nrneurol.2016.166
25. Bian W, Harter K, Hammond-Rosenbluth KE, Lupo JM, Xu D, Kelley DA, et al. A serial *in vivo* 7T magnetic resonance phase imaging study of white matter lesions in multiple sclerosis. *Mult Scler* 2013; **19**: 69–75. doi: https://doi.org/10.1177/1352458512447870
26. Absinta M, Sati P, Gaitán MI, Maggi P, Cortese ICM, Filippi M, et al. Seven-tesla phase imaging of acute multiple sclerosis lesions: A new window into the inflammatory process. *Ann Neurol* 2013; **74**: 669–78. doi: https://doi.org/10.1002/ana.23959
27. Absinta M, Sati P, Schindler M, Leibovitch EC, Ohayon J, Wu T, et al. Persistent 7-tesla phase rim predicts poor outcome in new multiple sclerosis patient lesions. *J Clin Invest* 2016; **126**: 2597–609. doi: https://doi.org/10.1172/JCI86198
28. Lupo JM, Li Y, Hess CP, Nelson SJ. Advances in ultra-high field MRI for the clinical management of patients with brain tumors. *Curr Opin Neurol* 2011; **24**: 605–15. doi: https://doi.org/10.1097/WCO.0b013e32834cd495
29. Provencher SW. Estimation of metabolite concentrations from localized in vivo proton NMR spectra. *Magn Reson Med* 1993; **30**: 672–9.
30. Srinivasan R, Ratiney H, Hammond-Rosenbluth KE, Pelletier D, Nelson SJ. MR spectroscopic imaging of glutathione in the white and gray matter at 7 T with an application to multiple sclerosis. *Magn Reson Imaging* 2010; **28**: 163–70. doi: https://doi.org/10.1016/j.mri.2009.06.008
31. Benjamin EJ, Virani SS, Callaway CW, Chamberlain AM, Chang AR, Cheng S, et al. Heart disease and stroke statistics-2018 update: a report from the American Heart Association. *Circulation* 2018; **137**: e67–e492. doi: https://doi.org/10.1161/CIR.0000000000000558
32. De Cocker LJ, Lindenholz A, Zwanenburg JJ, van der Kolk AG, Zwartbol M, Luijten PR, et al. Clinical vascular imaging in the brain at 7T. *Neuroimage* 2018; **168**: 452–8. doi: https://doi.org/10.1016/j.neuroimage.2016.11.044
33. Bae KT, Park S-H, Moon C-H, Kim J-H, Kaya D, Zhao T. Dual-echo arteriovenography imaging with 7T MRI. *Journal of Magnetic Resonance Imaging* 2010; **31**: 255–61. doi: https://doi.org/10.1002/jmri.22019
34. Kang C-K, Park C-A, Kim K-N, Hong S-M, Park C-W, Kim Y-B, et al. Non-invasive visualization of basilar artery perforators with 7T MR angiography. *Journal of Magnetic Resonance Imaging* 2010; **32**: 544–50. doi: https://doi.org/10.1002/jmri.22250
35. Zhu C, Haraldsson H, Tian B, Meisel K, Ko N, Lawton M, et al. High resolution imaging of the intracranial vessel wall at 3 and 7 T using 3D fast spin echo MRI. Magn Reson Mater Physics. *Biol Med* 2016; **29**: 559–70.
36. Fan Z, Yang Q, Deng Z, Li Y, Bi X, Song S, et al. Whole-brain intracranial vessel wall imaging at 3 Tesla using cerebrospinal fluid-attenuated T1-weighted 3D turbo spin echo. *Magn Reson Med* 2017; **77**: 1142–50. doi: https://doi.org/10.1002/mrm.26201
37. Zhang L, Zhang N, Wu J, Zhang L, Huang Y, Liu X, et al. High resolution three dimensional intracranial arterial wall imaging at 3 T using T1 weighted SPACE. *Magn Reson Imaging* . 2015; **33**: 1026–34. doi: https://doi.org/10.1016/j.mri.2015.06.006
38. SJ M, Yan L, Jann K, Wang DJJ. High Resolution Black-blood T1-weighted Turbo Spin Echo with Variable Flip Angles for Visualization of Small Perforating Arteries at 3 and 7 Tesla. In: *Proceedings of the Joint Annual Meeting ISMRM-ESMRMB*. Paris, France; 2018. pp. 5583.
39. Wrede KH, Dammann P, Mönninghoff C, Johst S, Maderwald S, Sandalcioglu IE, et al. Non-enhanced MR imaging of cerebral aneurysms: 7 Tesla versus 1.5 Tesla. *PLoS One* 2014; **9**: e84562–10. doi: https://doi.org/10.1371/journal.pone.0084562
40. Mönninghoff C, Maderwald S, Wanke I. Pre-interventional assessment of a vertebrobasilar aneurysm with 7 Tesla time-of-flight MR angiography. *RöFo - Fortschritte auf dem Gebiet der Röntgenstrahlen und der bildgebenden Verfahren* 2009; **181**: 266–8. doi: https://doi.org/10.1055/s-0028-1109110
41. Mönninghoff C, Maderwald S, Theysohn J, Kraff O, Ladd S, Ladd M, et al. Evaluation of Intracranial aneurysms with 7 T versus 1.5 T time-of-flight MR angiography – Initial experience. *RöFo - Fortschritte auf dem Gebiet der Röntgenstrahlen und der bildgebenden Verfahren* 2009; **181**: 16–23. doi: https://doi.org/10.1055/s-2008-1027863
42. Koning W, de Rotte AAJ, Bluemink JJ, van der Velden TA, Luijten PR, Klomp DWJ, et al. MRI of the carotid artery at 7 Tesla: Quantitative comparison with 3 Tesla. *Journal of Magnetic Resonance Imaging* 2015; **41**: 773–80. doi: https://doi.org/10.1002/jmri.24601
43. Lopez Gonzalez MR, Foo SY, Holmes WM, Stewart W, Muir KW, Condon B, et al. Atherosclerotic Carotid Plaque Composition: A 3T and 7T MRI-Histology Correlation Study. *J Neuroimaging* 2016; **26**: 406–13. doi: https://doi.org/10.1111/jon.12332
44. Novak V, Abduljalil AM, Novak P, Robitaille PM. High-resolution ultrahigh-field MRI of stroke. *Magn Reson Imaging* 2005; **23**: 539–48. doi: https://doi.org/10.1016/j.mri.2005.02.010
45. Pantoni L. Cerebral small vessel disease: from pathogenesis and clinical characteristics to therapeutic challenges. *Lancet Neurol* . 2010; **9**: 689–701. doi: https://doi.org/10.1016/S1474-4422(10)70104-6
46. Norrving B. Lacunar infarcts: no black holes in the brain are benign. *Pract Neurol* 2008; **8**: 222–8. doi: https://doi.org/10.1136/jnnp.2008.153601
47. Madai VI, von Samson-Himmelstjerna FC, Bauer M, Stengl KL, Mutke MA, Tovar-Martinez E, et al. Ultrahigh-field MRI in human ischemic stroke – a 7 tesla study. *PLoS One* 2012; **7**: e37631. doi: https://doi.org/10.1371/journal.pone.0037631
48. Bian W, Hess CP, Chang SM, Nelson SJ, Lupo JM. Susceptibility-weighted MR imaging of radiation therapy-induced cerebral microbleeds in patients with glioma:A comparison between 3T and 7T. *Neuroradiology* 2014; **56**: 91–6. doi: https://doi.org/10.1007/s00234-013-1297-8
49. Conijn MM, Geerlings MI, Biessels GJ, Takahara T, Witkamp TD, Zwanenburg JJ, et al. Cerebral microbleeds on MR imaging: comparison between 1.5 and 7T. *AJNR Am J Neuroradiol* 2011; **32**: 1043–9. doi: https://doi.org/10.3174/ajnr.A2450

50. Theysohn JM, Kraff O, Maderwald S, Barth M, Ladd SC, Forsting M, et al. 7 tesla MRI of microbleeds and white matter lesions as seen in vascular dementia. *Journal of Magnetic Resonance Imaging* 2011; **33**: 782–91. doi: https://doi.org/10.1002/jmri.22513
51. van Veluw SJ, Zwanenburg JJ, Engelen-Lee J, Spliet WG, Hendrikse J, Luijten PR, et al. *In* vivo detection of cerebral cortical microinfarcts with high-resolution 7T MRI. *J Cereb Blood Flow Metab* 2013; **33**: 322–9. doi: https://doi.org/10.1038/jcbfm.2012.196
52. Siero JCW, Hermes D, Hoogduin H, Luijten PR, Ramsey NF, Petridou N. BOLD matches neuronal activity at the mm scale: A combined 7T fMRI and ECoG study in human sensorimotor cortex. *Neuroimage* . 2014; **101**: 177–84. doi: https://doi.org/10.1016/j.neuroimage.2014.07.002
53. Koopmans PJ, Barth M, Orzada S, Norris DG. Multi-echo fMRI of the cortical laminae in humans at 7 T. *Neuroimage* 2011; **56**: 1276–85. doi: https://doi.org/10.1016/j.neuroimage.2011.02.042
54. Siero JC, Hendrikse J, Hoogduin H, Petridou N, Luijten P, Donahue MJ. Cortical depth dependence of the BOLD initial dip and poststimulus undershoot in human visual cortex at 7 Tesla. *Magn Reson Med* 2015; **73**: 2283–95. doi: https://doi.org/10.1002/mrm.25349
55. De Martino F, Zimmermann J, Muckli L, Ugurbil K, Yacoub E, Goebel R. Cortical depth dependent functional responses in humans at 7T: improved specificity with 3D GRASE. *PLoS One* 2013; **8**: e60514–2. doi: https://doi.org/10.1371/journal.pone.0060514
56. Kang CK, Wörz S, Liao W, Park CA, Kim YB, Park CW, et al. Three dimensional model-based analysis of the lenticulostriate arteries and identification of the vessels correlated to the infarct area: preliminary results. *Int J Stroke* 2012; **7**: 558–63. doi: https://doi.org/10.1111/j.1747-4949.2011.00611.x
57. Ostrom QT, Gittleman H, Liao P, Vecchione-Koval T, Wolinsky Y, Kruchko C, et al. CBTRUS statistical report: Primary brain and other central nervous system tumors diagnosed in the United States in 2010-2014. *Neuro Oncol* 2017; **19**(Suppl_5): v1–v88. doi: https://doi.org/10.1093/neuonc/nox158
58. Elkhaled A, Jalbert L, Yoshihara H, Bourne G, Cloyd C, Phillips J. *Comparison of glioma sub-populations using in-vivo ADC values and ex-vivo 1 H HR-MAS spectroscopy Proceedings of the 18th Annual Meeting of ISMRM*. Stockholm, Sweden; 2010. pp. 2203.
59. Srinivasan R, Phillips JJ, Vandenberg SR, Polley MY, Bourne G, Au A, et al. Ex vivo MR spectroscopic measure differentiates tumor from treatment effects in GBM. *Neuro Oncol* 2010; **12**: 1152–61. doi: https://doi.org/10.1093/neuonc/noq075
60. Li Y, Larson P, Chen AP, Lupo JM, Ozhinsky E, Kelley D, et al. Short-echo three-dimensional H-1 MR spectroscopic imaging of patients with glioma at 7 Tesla for characterization of differences in metabolite levels. *J Magn Reson Imaging* 2015; **41**: 1332–41. doi: https://doi.org/10.1002/jmri.24672
61. Verma G, Mohan S, Nasrallah MP, Brem S, Lee JYK, Chawla S, et al. Non-invasive detection of 2-hydroxyglutarate in IDH-mutated gliomas using two-dimensional localized correlation spectroscopy (2D L-COSY) at 7 Tesla. *J Transl Med* 2016; **14**: 1–8. doi: https://doi.org/10.1186/s12967-016-1035-1
62. Dashner RA, Chakeres DW, Kangarlu A, Schmalbrock P, Christoforidis GA, DePhilip RM. MR imaging visualization of the cerebral microvasculature: A comparison of live and postmortem studies at 8 T. *AJNR Am J Neuroradiol* 2003; **24**: 1881–4.
63. WTC Y, Christoforidis GA, Koch RM, Sammet S, Schmalbrock P, Yang M, et al. Clinical magnetic resonance imaging of brain tumors at ultrahigh field: A state-of-the-art review. *Top Magn Reson Imaging* . 2006; **17**: 53–61.
64. Birner P, Piribauer M, Fischer I, Gatterbauer B, Marosi C, Ambros PF, et al. Vascular patterns in glioblastoma influence clinical outcome and associate with variable expression of angiogenic proteins: evidence for distinct angiogenic subtypes. *Brain Pathol* 2003; **13**: 133–43. doi: https://doi.org/10.1111/j.1750-3639.2003.tb00013.x
65. Louis DN, Ohgaki H, Wiestler OD, Cavenee WK, Burger PC, Jouvet A, et al. The 2007 WHO classification of tumours of the central nervous system. *Acta Neuropathol* 2007; **114**: 97–109. doi: https://doi.org/10.1007/s00401-007-0243-4
66. Di Ieva A, Göd S, Grabner G, Grizzi F, Sherif C, Matula C, et al. Three-dimensional susceptibility-weighted imaging at 7 T using fractal-based quantitative analysis to grade gliomas. *Neuroradiology* 2013; **55**: 35–40. doi: https://doi.org/10.1007/s00234-012-1081-1
67. Grabner G, Nöbauer I, Elandt K, Kronnerwetter C, Woehrer A, Marosi C, et al. Longitudinal brain imaging of five malignant glioma patients treated with bevacizumab using susceptibility-weighted magnetic resonance imaging at 7 T. *Magn Reson Imaging* 2012; **30**: 139–47. doi: https://doi.org/10.1016/j.mri.2011.08.004
68. Moenninghoff C, Maderwald S, Theysohn JM, Kraff O, Ladd ME, El Hindy N, et al. Imaging of adult astrocytic brain tumours with 7 T MRI: preliminary results. *Eur Radiol* 2010; **20**: 704–13. doi: https://doi.org/10.1007/s00330-009-1592-2
69. Guy RL, Benn JJ, Ayers AB, Bingham JB, Lowy C, Cox TC, et al. A comparison of CT and MRI in the assessment of the pituitary and parasellar region. *Clin Radiol* 1991; **43**: 156–61. doi: https://doi.org/10.1016/S0009-9260(05)80470-2
70. Ludecke D, Flitsch J, Knappe U, Saeger W. Cushing' s disease: a surgical view. *J Neurooncol* 2001; **5**: 151–66.
71. Newell-Price J, Trainer P, Besser M, Grossman A. The diagnosis and differential diagnosis of Cushing's syndrome and pseudo-Cushing's states. *Endocr Rev* 1998; **19**: 647–72. doi: https://doi.org/10.1210/edrv.19.5.0346
72. Nieman LK, Biller BM, Findling JW, Newell-Price J, Savage MO, Stewart PM, et al. The diagnosis of Cushing's syndrome: an Endocrine Society Clinical Practice Guideline. *J Clin Endocrinol Metab* 2008; **93**: 1526–40. doi: https://doi.org/10.1210/jc.2008-0125
73. de Rotte AAJ, Groenewegen A, Rutgers DR, Witkamp T, Zelissen PMJ, Meijer FJA, et al. High resolution pituitary gland MRI at 7.0 tesla: a clinical evaluation in Cushing's disease. *Eur Radiol* 2016; **26**: 271–7. doi: https://doi.org/10.1007/s00330-015-3809-x
74. Law M, Wang R, C-SJ L, Shiroishi MS, Carmichael JD, Mack WJ. Value of pituitary gland MRI at 7 T in Cushing's disease and relationship to inferior petrosal sinus sampling: case report. *J Neurosurg* 2018; **23**: 1–5. doi: https://doi.org/10.3171/2017.9.JNS171969
75. Mönninghoff C, Maderwald S, Theysohn J, Schütt P, Gauler T, Kraff O, et al. Imaging of Brain Metastases of Bronchial Carcinomas with 7 T MRI – Initial Results. *RöFo - Fortschritte auf dem Gebiet der Röntgenstrahlen und der bildgebenden Verfahren* 2010; **182**: 764–72. doi: https://doi.org/10.1055/s-0029-1245440
76. Obusez EC, Lowe M, Oh SH, Wang I, Jennifer B, Ruggieri P, Bullen J, et al. 7T MR of intracranial pathology: Preliminary observations and comparisons to 3T and 1.5T. *Neuroimage* 2018; **168**: 459–76. doi: https://doi.org/10.1016/j.neuroimage.2016.11.030

77. Kwan P, Brodie MJ. Early identification of refractory epilepsy. *N Engl J Med* 2000; **342**: 314–9. doi: https://doi.org/10.1056/NEJM200002033420503
78. Wiebe S. Brain surgery for epilepsy. *The Lancet* 2003; **362**: s48–s49. doi: https://doi.org/10.1016/S0140-6736(03)15075-1
79. Téllez-Zenteno JF, Hernández Ronquillo L, Moien-Afshari F, Wiebe S. Surgical outcomes in lesional and non-lesional epilepsy: a systematic review and meta-analysis. *Epilepsy Res* 2010; **89**(2-3): 310–8. doi: https://doi.org/10.1016/j.eplepsyres.2010.02.007
80. Duncan JS. Imaging in the surgical treatment of epilepsy. *Nat Rev Neurol* 2010; **6**: 537–50. doi: https://doi.org/10.1038/nrneurol.2010.131
81. De Ciantis A, Barba C, Tassi L, Cosottini M, Tosetti M, Costagli M, et al. 7T MRI in focal epilepsy with unrevealing conventional field strength imaging. *Epilepsia* 2016; **57**: 445–54. doi: https://doi.org/10.1111/epi.13313
82. De Ciantis A, Barkovich AJ, Cosottini M, Barba C, Montanaro D, Costagli M, et al. Ultra-high-field MR imaging in polymicrogyria and epilepsy. *AJNR Am J Neuroradiol* 2015; **36**: 309–16. doi: https://doi.org/10.3174/ajnr.A4116
83. Guerrini R, Dobyns WB, Barkovich AJ. Abnormal development of the human cerebral cortex: genetics, functional consequences and treatment options. *Trends Neurosci* 2008; **31**: 154–62. doi: https://doi.org/10.1016/j.tins.2007.12.004
84. Feldman RE, Rutland JW, Fields MC, Marcuse LV, Pawha PS, Delman BN, et al. Quantification of perivascular spaces at 7T: A potential MRI biomarker for epilepsy. *Seizure* 2018; **54**: 11–18. doi: https://doi.org/10.1016/j.seizure.2017.11.004
85. Springer E, Dymerska B, Cardoso PL, Robinson SD, Weisstanner C, Wiest R, et al. Comparison of routine brain imaging at 3 T and 7 T. *Invest Radiol* 2016; **51**: 469–82. doi: https://doi.org/10.1097/RLI.0000000000000256
86. Blümcke I, Thom M, Aronica E, Armstrong DD, Bartolomei F, Bernasconi A, et al. International consensus classification of hippocampal sclerosis in temporal lobe epilepsy: A task force report from the ILAE commission on diagnostic methods. *Epilepsia* 2013; **54**: 1315–29. doi: https://doi.org/10.1111/epi.12220
87. Huang C-W, Hsieh Y-J, Tsai J-J, Pai M-C. Cognitive performance in cryptogenic epilepsy. *Acta Neurol Scand* 2005; **112**: 228–33. doi: https://doi.org/10.1111/j.1600-0404.2005.00480.x
88. Frischer JM, Göd S, Gruber A, Saringer W, Grabner G, Gatterbauer B, et al. Susceptibility-weighted imaging at 7T: Improved diagnosis of cerebral cavernous malformations and associated developmental venous anomalies. *Neuroimage* 2012; **1**: 116–20. doi: https://doi.org/10.1016/j.nicl.2012.09.005
89. Schlamann M, Maderwald S, Becker W, Kraff O, Theysohn JM, Mueller O, et al. Cerebral cavernous hemangiomas at 7 Tesla: initial experience. *Acad Radiol* 2010; **17**: 3–6. doi: https://doi.org/10.1016/j.acra.2009.10.001
90. Prince M, Bryce R, Albanese E, Wimo A, Ribeiro W, Ferri CP. The global prevalence of dementia: A systematic review and metaanalysis. *Alzheimer's & Dementia* 2013; **9**: 63–75. doi: https://doi.org/10.1016/j.jalz.2012.11.007
91. Alzheimer's Association Alzheimer's disease facts and figures. *Alzheimer's Dement* 20102010; **6**: 158–94; **6**: 158–94.
92. Frozza RL, Lourenco MV, De Felice FG. Challenges for alzheimer's disease therapy: Insights from novel mechanisms beyond memory defects. *Front Neurosci* 2018; **12**: 1–13. doi: https://doi.org/10.3389/fnins.2018.00037
93. Theysohn JM, Kraff O, Maderwald S, Schlamann MU, de Greiff A, Forsting M, et al. The human hippocampus at 7 T-In vivo MRI. *Hippocampus* 2009; **19**: 1–7. doi: https://doi.org/10.1002/hipo.20487
94. Kerchner GA, Hess CP, Hammond-Rosenbluth KE, Xu D, Rabinovici GD, Kelley DAC, et al. Hippocampal CA1 apical neuropil atrophy in mild alzheimer disease visualized with 7-T MRI. *Neurology* 2010; **75**: 1381–7. doi: https://doi.org/10.1212/WNL.0b013e3181f736a1
95. Boutet C, Chupin M, Lehéricy S, Marrakchi-Kacem L, Epelbaum S, Poupon C, et al. Detection of volume loss in hippocampal layers in Alzheimer's disease using 7 T MRI: A feasibility study. *Neuroimage* 2014; **5**: 341–8. doi: https://doi.org/10.1016/j.nicl.2014.07.011
96. Wisse LEM, Biessels GJ, Heringa SM, Kuijf HJ, Koek Dineke (H.) L., Luijten PR, et al. Hippocampal subfield volumes at 7T in early Alzheimer's disease and normal aging. *Neurobiol Aging* . 2014; **35**: 2039–45. doi: https://doi.org/10.1016/j.neurobiolaging.2014.02.021
97. Sepehrband F, Wang DJ, Toga AW. Revealing small subfields of hippocampus in vivo with 7T structural MRI. In: *Proceedings of the Alzhemer's Imaging Consortium*. Chicago, Illinois; 2018.
98. Pipe JG. Motion correction with PROPELLER MRI: application to head motion and free-breathing cardiac imaging. *Magn Reson Med* 1999; **42**: 963–9.
99. van Rooden S, Maat-Schieman ML, Nabuurs RJ, van der Weerd L, van Duijn S, van Duinen SG, et al. Cerebral amyloidosis: postmortem detection with human 7.0-T MR imaging system. *Radiology* 2009; **253**: 788–96. doi: https://doi.org/10.1148/radiol.2533090490
100. Zeineh MM, Chen Y, Kitzler HH, Hammond R, Vogel H, Rutt BK. Activated iron-containing microglia in the human hippocampus identified by magnetic resonance imaging in Alzheimer disease. *Neurobiol Aging* 2015; **36**: 2483–500. doi: https://doi.org/10.1016/j.neurobiolaging.2015.05.022
101. van Veluw SJ, Biessels GJ, Bouvy WH, Spliet WG, Zwanenburg JJ, Luijten PR, et al. Cerebral amyloid angiopathy severity is linked to dilation of juxtacortical perivascular spaces. *J Cereb Blood Flow Metab* 2016; **36**: 576–80. doi: https://doi.org/10.1177/0271678X15620434
102. Cai K, Tain R, Das S, Damen FC, Sui Y, Valyi-Nagy T, et al. The feasibility of quantitative MRI of perivascular spaces at 7T. *J Neurosci Methods* 2015; **256**: 151–6. doi: https://doi.org/10.1016/j.jneumeth.2015.09.001
103. Kantarci K, Murray ME, Schwarz CG, Reid RI, Przybelski SA, Lesnick T, et al. White-matter integrity on DTI and the pathologic staging of Alzheimer's disease. *Neurobiol Aging* . 2017; **56**: 172–9. doi: https://doi.org/10.1016/j.neurobiolaging.2017.04.024
104. Gulban OF, De Martino F, Vu AT, Yacoub E, Uğurbil K, Lenglet C. Cortical fibers orientation mapping using in-vivo whole brain 7 T diffusion MRI. *Neuroimage* . 2018; **178**: 104–. doi: https://doi.org/10.1016/j.neuroimage.2018.05.010
105. AT V, Auerbach E, Lenglet C, Moeller S, Sotiropoulos SN, Jbabdi S, et al. High resolution whole brain diffusion imaging at 7T for the human connectome project. *Neuroimage* 2015; **122**: 318–31.
106. Jenkinson M, Beckmann CF, Behrens TE, Woolrich MW, Smith SM. FSL. *Neuroimage* 2012; **62**: 782–90.
107. Cabeen RP, Laidlaw DH, Toga AW. Quantitative Imaging Toolkit: Software for Interactive 3DVisualization, Data Exploration, and Computational Analysis of Neuroimaging Datasets. *In:Proceedings of the Joint Annual Meeting ISMRM-ESMRMB. Paris, France; 2018. pp. 8882.*
108. Cabeen RP, Bastin ME, Laidlaw DH. Kernel regression estimation of fiber orientation

mixtures in diffusion MRI. *Neuroimage* 2016; **127**: 158–72.
109. Sepehrband F, O'Brien K, Barth M, O'Brien K. A time-efficient acquisition protocol for multipurpose diffusion-weighted microstructural imaging at 7 Tesla. *Magn Reson Med* 2017; **78**: 2170–84. doi: https://doi.org/10.1002/mrm.26608
110. Nussbaum RL, Ellis CE. Alzheimer's Disease and Parkinson's Disease. *N Engl J Med Overseas Ed* 2003; **348**: 1356–64. doi: https://doi.org/10.1056/NEJM2003ra020003
111. Hoehn MM, Yahr MD. Parkinsonism: onset, progression and mortality. *Neurology* 1967; **17**: 427–42. doi: https://doi.org/10.1212/WNL.17.5.427
112. Pollanen MS, Dickson DW, Bergeron C. Pathology and biology of the Lewy body. *J Neuropathol Exp Neurol* 1993; **52**: 183–91. doi: https://doi.org/10.1097/00005072-199305000-00001
113. Cosottini M, Frosini D, Pesaresi I, Costagli M, Biagi L, Ceravolo R, et al. MR imaging of the substantia nigra at 7 T enables diagnosis of Parkinson disease. *Radiology* 2014; **271**: 831–8. doi: https://doi.org/10.1148/radiol.14131448
114. Schuepbach WM, Rau J, Knudsen K, Volkmann J, Krack P, Timmermann L, et al. Neurostimulation for parkinson's disease with early motor complications. *N Engl J Med* 2013; **368**: 610–22. doi: https://doi.org/10.1056/NEJMoa1205158
115. Welter ML, Schüpbach M, Czernecki V, Karachi C, Fernandez-Vidal S, Golmard JL, et al. Optimal target localization for subthalamic stimulation in patients with parkinson disease. *Neurology* 2014; **82**: 1352–61. doi: https://doi.org/10.1212/WNL.0000000000000315
116. Plantinga BR, Temel Y, Duchin Y, Uludağ K, Patriat R, Roebroeck A, et al. Individualized parcellation of the subthalamic nucleus in patients with Parkinson's disease with 7T MRI. *Neuroimage* 2018; **168**: 403–11. doi: https://doi.org/10.1016/j.neuroimage.2016.09.023
117. Lenglet C, Abosch A, Yacoub E, De Martino F, Sapiro G, Harel N. Comprehensive in vivo mapping of the human basal ganglia and thalamic connectome in individuals using 7T MRI. *PLoS One* 2012; **7**: e29153. doi: https://doi.org/10.1371/journal.pone.0029153
118. Abosch A, Yacoub E, Ugurbil K, Harel N. An assessment of current brain targets for deep brain stimulation surgery with susceptibility-weighted imaging at 7 tesla. *Neurosurgery* 2010; **67**: 1745–56. doi: https://doi.org/10.1227/NEU.0b013e3181f74105
119. Cho ZH, Min HK, Oh SH, Han JY, Park CW, Chi JG, et al. Direct visualization of deep brain stimulation targets in Parkinson disease with the use of 7-tesla magnetic resonance imaging. *J Neurosurg* 2010; **113**: 639–47. doi: https://doi.org/10.3171/2010.3.JNS091385
120. Chandran AS, Bynevelt M, Lind CR. Magnetic resonance imaging of the subthalamic nucleus for deep brain stimulation. *J Neurosurg* 2016; **124**: 96–105. doi: https://doi.org/10.3171/2015.1.JNS142066
121. Pan JW, Lo KM, Hetherington HP. Role of very high order and degree B0 shimming for spectroscopic imaging of the human brain at 7 tesla. *Magn Reson Med* . 2012; **68**: 1007–17. doi: https://doi.org/10.1002/mrm.24122
122. Heidemann RM, Porter DA, Anwander A, Feiweier T, Heberlein K, Knösche TR, et al. Diffusion imaging in humans at 7T using readout-segmented EPI and GRAPPA. *Magn Reson Med* 2010; **64**: 9–14. doi: https://doi.org/10.1002/mrm.22480
123. Ibrahim TS, Lee R, Baertlein BA, Abduljalil AM, Zhu H, Robitaille PM. Effect of RF coil excitation on field inhomogeneity at ultra high fields: a field optimized TEM resonator. *Magn Reson Imaging* 2001; **19**: 1339–47. doi: https://doi.org/10.1016/S0730-725X(01)00404-0
124. Tannús A, Garwood M. Adiabatic pulses. *NMR Biomed* 1997; **10**: 423–34. doi: https://doi.org/10.1002/(SICI)1099-1492(199712)10:8<423::AID-NBM488>3.0.CO;2-X
125. Zhu Y. Parallel excitation with an array of transmit coils. *Magn Reson Med* 2004; **51**: 775–84. doi: https://doi.org/10.1002/mrm.20011
126. Barry RL, Vannesjo SJ, By S, Gore JC, Smith SA. Spinal cord MRI at 7T. *Neuroimage* 2018; **168**: 437–51. doi: https://doi.org/10.1016/j.neuroimage.2017.07.003
127. Zaitsev M, Maclaren J, Herbst M. Motion artifacts in MRI: A complex problem with many partial solutions. *J Magn Reson Imaging* 2015; **42**: 887–901. doi: https://doi.org/10.1002/jmri.24850
128. Herbst M, Maclaren J, Lovell-Smith C, Sostheim R, Egger K, Harloff A, et al. Reproduction of motion artifacts for performance analysis of prospective motion correction in MRI. *Magn Reson Med* 2014; **71**: 182–90. doi: https://doi.org/10.1002/mrm.24645
129. Stucht D, Danishad KA, Schulze P, Godenschweger F, Zaitsev M, Speck O. Highest resolution in vivo human brain MRI using prospective motion correction. *PLoS One* 2015; **10**: e0133921–17. doi: https://doi.org/10.1371/journal.pone.0133921
130. Sammet CL, Yang X, Wassenaar PA, Bourekas EC, Yuh BA, Shellock F, et al. RF-related heating assessment of extracranial neurosurgical implants at 7T. *Magn Reson Imaging* 2013; **31**: 1029–34. doi: https://doi.org/10.1016/j.mri.2012.10.025
131. Dula AN, Virostko J, Shellock FG. Assessment of MRI issues at 7 T for 28 implants and other objects. *AJR Am J Roentgenol* 2014; **202**: 401–5. doi: https://doi.org/10.2214/AJR.13.10777
132. Feng DX, McCauley JP, Morgan-Curtis FK, Salam RA, Pennell DR, Loveless ME, et al. Evaluation of 39 medical implants at 7.0 T. *Br J Radiol* 2015; **88**: 20150633–10. doi: https://doi.org/10.1259/bjr.20150633
133. Setsompop K, Feinberg DA, Polimeni JR. Rapid brain MRI acquisition techniques at ultra-high fields. *NMR Biomed* 2016; **29**: 1198–221. doi: https://doi.org/10.1002/nbm.3478